SSRG International Journal of Electrical and Electronics Engineering
ISSN: 2348-8379/ https://doi.org/10.14445/23488379/IJEEE-V11I2P112

Volume 11 Issue 2, 107-118, February 2024

Original Article

A Double-Slotted Microstrip Rectangular 6x6 Array for Sub-6 GHz Wireless Applications

Fahmida Hossain[1], Mohd Khanapiah Bin Nor[1], A.K.M. Zakir Hossain[1*], Nurulhalim Bin Hassim[1]

[1]*Centre for Telecommunication Research & Innovation (CeTRI), Electronics and Computer Engineering Technology (FTKEK), Technical University of Malaysia Malacca (UTeM), Malacca, Malaysia.*

[*]*Corresponding Author : zakir@utem.edu.my*

Received: 22 November 2023 Revised: 15 December 2023 Accepted: 22 January 2024 Published: 16 February 2024

Abstract *- In this article, a double-slotted microstrip rectangular 6×6 MIMO array antenna is proposed with an intention for the sub-6 GHz smartphone and wireless applications. In this proposed design, the Partial Ground Plane (PGP) technique is applied to the Single-Element Antenna (SEA) design to achieve an Ultra-Wideband (UWB) response of 1.43GHz. The design works within 3.1 to 4.53 GHz of -10 dB S-parameter bandwidth (BW). The SEA has a small dimensions of only 40 × 30 mm² and a 0.508 mm thickness. Moreover, the 6-element array aligns with 6.6-inch display smartphones by having a final dimension of 75 × 150 mm². The MIMO performance parameters of this proposed design have a good isolation of below -16.6 dB between the ports. Furthermore, the maximum Realized Gain (RG) of 5.44 dBi, and a Total antenna Efficiency (TE) of as high as 80% are achieved by simulation and also validated through measurement. Likewise, the Envelope Correlation Coefficient (ECC) of this MIMO array stays consistently below 0.004 and has a Diversity Gain (DG) of more than 9.98 throughout the entire BW. Additionally, the Specific Absorption Rate (SAR) analysis with Hand-Head phantom reveals a remarkable result of as low as 0.094 W/kg for 10g mass at port 2, whereby the value never goes higher than 0.413 W/kg at any port that ensures compliance with MIMO standards for smartphone applications.*

Keywords *- ECC, MIMO, PGP, RG, Wireless.*

1. Introduction

The deployment of the Fifth Generation (5G) wireless technology has brought many significant advancements in wireless communications, such as reduced latency, improved connectivity, remarkable data transfer rate, etc. [1]. Moreover, the allocations for 5G frequency bands have been offered differently in different countries. However, broadly, it has two categories: the sub-6 GHz band (0.45 GHz to 6 GHz) and the millimeter-wave (mm-wave) frequency range (24.25 GHz to 52.6 GHz). Additionally, within the sub-6 GHz range, three key segments exist: i) the lower-band (700 MHz), ii) the mid-band (3.4 GHz to 3.6 GHz), and iii) the high-band (4.8 GHz to 6 GHz). The lower frequencies are utilized for wider area coverage, whereby the mmWave bands are used to unlock the high data speeds; however, they work for short distances only [2].

Yet, these 5G frequency bands have presented a distinctive challenge, the necessity to redesign crucial hardware elements within wireless cellular communication systems. Among these elements, Base Transceiver Stations (BTS) and mobile handsets must undergo substantial alterations to align with the particular frequency demands set by various countries. In this intricate landscape of wireless communication, the antenna takes center stage, acting as the critical gateway device responsible for transmitting and receiving signals. When addressing the development of MIMO antenna arrays for smartphones, a formidable challenge arises in fitting these arrays into the often-limited spaces provided in mobile devices [2]. Several factors create challenges for the MIMO designers while proposing MIMO arrays in 5G bands for smartphones, such as the number of antenna elements they incorporate, whether they employ isolation circuitry, their operational mode, and the specific configuration of the antenna structure. Therefore, while designing the MIMO array for smartphones, a careful balance is necessary between the regulated number of elements, operational Bandwidth (BW), minimal isolation, and an optimum structural design. Yet, this is still a considerable challenge for the MIMO designers.

To deal with the issues mentioned above for enhancing the performance of the 5G smartphones, the incorporation of a reconfigurable MIMO array comprising two antenna elements (2×2 MIMO) is proposed in [3]. This proposal is made based on the meander lines as radiating elements of the

MIMO, which are connected/disconnected electronically from the 50Ω microstrip feedline to achieve reconfigurability. The authors considered two radiating arms per Single Elements Antenna (SEA) design. This reconfigurable capability introduces valuable frequency diversity, allowing operation at 2.4/3.5 GHz. Remarkably, at these frequencies, the ECC measures a mere 0.0056 and 0.0009, correspondingly highlighting the effectiveness of this design. However, it's worth noting that this antenna array achieves a very low minimum isolation level of 12 dB and operates with certain limitations.

Similarly, in [4], specifically for mobile phone applications, a dual-element MIMO antenna array is proposed. This particular antenna offers good coverage for both bands at 3.5 & 4.3 GHz with a span as wide as 400 MHz. Furthermore, its capabilities extend to higher frequencies, including those up to 12 GHz BW within the mmWave 5G bands, which operate in the range between 24 GHz and 38 GHz. For the bands below 6 GHz, this antenna achieves a substantial isolation level of as high as 21 dB, whereas for the mmWave, it attains an isolation of 24 dB. Complementary metamaterial techniques are utilized here, and they are strategically positioned between each antenna to achieve these results. Of significant note, the ECC for this advanced antenna array consistently remains below 0.05.

The prevalence of four-port MIMO antenna arrays is gaining significant traction in both research and industry domains, particularly in the context of 5G smartphones, due to their outstanding performance capabilities. In accordance with [5], a proposal is made with a 4×4 MIMO array antenna for integration into 5G mobile devices that work for dual-band of distinct frequency ranges: 3.4 GHz -3.6 GHz and 4.8 GHz - 5.0 GHz, displaying a minimum level of isolation as low as -17.5 dB. However, it's worth noting that this array exhibits a relatively modest efficiency of only 60% and maintains an ECC of as low as 0.05 across both of the bands.

For similar frequency bands, another proposal presented in [6] features a 4×4 MIMO configuration. This array functions well with 200 MHz BW for both of the bands. However, its performance gets curtailed as it can achieve a Total Efficiency (TE) of 70% only, accompanied by low isolation of a mere 16.5 dB, and no SAR analysis is included.

In [7], an alternative method is presented, featuring a 4×4 MIMO array designed for 5G mobile devices that possess dual operational band capability and along with diversity. The planar dipoles are used as SEA in this proposal. This array showcases an ECC as low as 0.005; however, it dents its performance as the minimum isolation level is only -15 dB. Additionally, this proposal provides a good analysis of the SAR, examining the interaction of the array placed on top of the head-hand phantom. Once more, the TE stands at only 51% for the antenna at port 1.

Furthermore, the paper delivers a comprehensive SAR analysis, investigating the array's interaction with the human head and hand, yielding a result of 1.7W/Kg at 3.5GHz. In summary, the growing adoption of four-port MIMO arrays for smartphones for 5G is a promising trend among both researchers and industrial engineers.

In recent times, researchers have explored various approaches to propose innovative designs for MIMO array antennas with different element counts - six [8, 9], eight [10-13], ten [14], and twelve [15, 16] - to enhance MIMO performance for below 6 GHz frequencies for 5G communications in handphones. In [8], the authors have proposed a 6×6 MIMO array with space and pattern diversity. The array has achieved a good ECC of 0.005. The isolation and the SAR values are also within acceptable range. However, the design's performance falls short by delivering the TE of a mere 51% only. Similarly, in [9], a six-element MIMO array operating below 2.5 GHz was introduced, utilizing a slotted technique for resonance, parasitic elements for enhanced isolation, and a modified ground structure. Despite achieving a maximum isolation of 45 dB, the minimum isolation degraded to 12 dB. However, no specific SAR analysis was presented for mobile phone applications.

In [10], an eight-element (8×8) array designed for the 3.5 GHz 5G band on an FR4 substrate was proposed. This design featured a modified rectangular-slotted ground plane with antennas placed side by side, meeting acceptable standards for in-band resonance dip and ECC. Nevertheless, isolation remained a challenge, reaching barely -12 dB, and no SAR analysis was provided for smartphone applications. Another proposal in [11] introduced a design using dual-polarized Self-Complementary Antennas (SCA) with edge corner probe-feed technique at 3.6 GHz, achieving high gain, improved radiation coverage, and an acceptable SAR value. However, isolation between ports 1 and 2 (S21) was less than -12 dB, and ECC was surprisingly very high.

In [12], an 8-element MIMO array designed for 5G smartphones employed Deep Learning (DL) for antenna dimension estimation, achieving efficient results but falling short of the -15 dB benchmark for isolation. Similarly, [13] presented an 8-element array operating between 3.6-4.7 GHz with an open L-slot on the ground plane, yielding a favorable ECC but suboptimal port-to-port isolation.

Moving to a 10-element array in [14], the slotted Ground Plane (GP) technique was utilized for resonance and isolation. While achieving a good SAR value and ECC, the port-to-port isolation was merely -11 dB, below MIMO standards. [15] and [16] proposed 12-element MIMO arrays for 5G smartphones at 3.5 GHz, employing a side edge positioning technique for MIMO performance. However, both designs suffered from low isolation, decreased TE, high ECC, and lacked SAR analysis. The summary can be seen in Table 1.

Table 1. State of the art in recent proposed MIMO array antennas for smartphone

Method Utilized	Isolation (dB)	ECC	TE (%)	SAR, W/Kg
Metamaterial Unit Cells [4]	-21	0.05	50	Na
Side Edge Positioning [6]	-17.5	0.05	60	Na
Parasitic Rectangle Strip [7]	-16.5	0.01	70	Na
Space and Pattern Diversity [8]	-15	0.005	51	1.7
Parasitic Patch and Slotted GP [9]	-12	0.002	88	Na
Slotted GP [10]	-12	0.03	70	Na
Edge Corner Probe-Feed [11]	-12	0.004	70	1.8
DL [12]	-12.5	0.1	Na	Na
L-Slotted GP [13]	-11	0.08	87	Na
Slotted GP [14]	-11	0.07	65	1.28
Side Edge Positioning [15]	-12	0.42	39	Na
Side Edge Positioning [16]	-10	0.4	36	Na
PGP and 90° Sequentially Rotation (This Work)	**-20**	**0.004**	**71**	**0.094**

It's evident from the previous proposals available that some of them excel in specific performance parameters while others fall short. Some designs demonstrate strong isolation but exhibit lower ECC or efficiency parameters, among other considerations. Furthermore, many of these proposals are intended for implementation in smartphones, yet they often lack adequate SAR analysis.

To address these issues within the context of this article, a proposal is put forth to design and develop a 6 × 6 element MIMO array. This array features a modified rectangular monopole antenna configuration, specifically tailored to meet the intricate communication requirements of 5G mobile phones. The subsequent sections (2) of this article delve into the design and synthesis of both Single-Element Antennas (SEA) and the 6 × 6 MIMO array. Section 3 provides an in-depth exploration of the performance characteristics of these antenna configurations, accompanied by relevant graphical representations. The article concludes in Section 4, summarizing the proposed work.

2. Design of Antenna and Array

Figure 1 illustrates the design layout and the detailed dimensions of the suggested SEA. The proposed antenna was designed and simulated using CST-MWS 2023. Expressly, Figure 1(a), and 1(b) represent the front and the rear perspectives of the simulated SEA, while Figure 1(c), and 1(d) display the front and back aspects of the physically fabricated model, respectively. The Rogers RT-5880 is chosen as the dielectric substrate material for this design. The design is manufactured using an etching process.

The SEA design incorporates a modified rectangular patch, an attached transmission line to the feed, and two similar dimensioned rectangular slots of 6.85×1.1 mm2 in size, positioned at the top left and bottom right edges of the top radiating patch. All the dimensions of the rectangular patch (length and width) are estimated by Equations (1) and (2), respectively [15, 16], and later optimized in CST-MWS.

Where, C_0 represents the speed of light in a vacuum, ε_r & ε_e are the relative and effective dielectric constants, respectively, h represents the substrate thickness, fc is the resonant frequency and $F = \frac{8.791 \times 10^9}{f_c\sqrt{\varepsilon_r}}$.

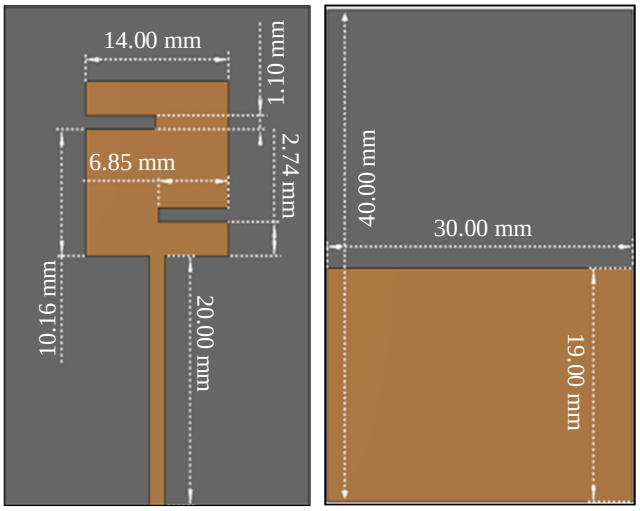

(a) SEA front layout **(b) SEA back layout**

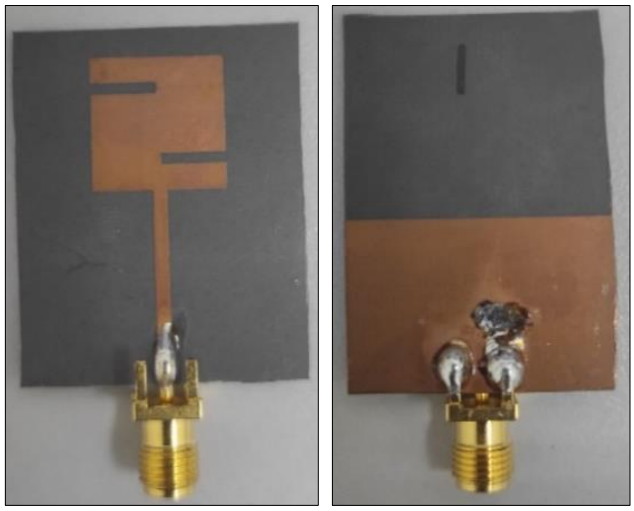

(c) SEA front (fabricated) (d) SEA Back (fabricated)

Fig. 1 SEA design and layout

Hence, the total antenna Length (L) and the Width (W) are obtained as 14 mm each. Likewise, the slot length and the width are also optimized by the CST-MWS software. Also, the microstrip feedline length is kept the same as the antenna width. Again, the optimized antenna dimension is obtained as 40×30 mm^2 after optimizing in CST-MWS.

The design steps are illustrated in Figure 2. At the start, a primary rectangular microstrip patch antenna with a Full-Ground Plane (FGP) was simulated. After that (second stage), two rectangular slots were introduced, maintaining the FGP. In the final stage, the FGP is shortened to create a PGP bottom patch to increase the operational BW of the antenna.

$$W = \frac{C_0}{2f_c\sqrt{\frac{(\varepsilon_r+1)}{2}}} \quad (1)$$

$$L = \frac{C_0}{2f_c\sqrt{\varepsilon_e}} - 0.824h\frac{(\varepsilon_e+0.3)(\frac{W_k}{h}+0.264)}{(\varepsilon_e-0.258)(\frac{W_k}{h}+0.8)} \quad (2)$$

Figure 3 provides a comprehensive view of our 6×6 MIMO antenna design. Figure 3(a), and Figure 3(b) offers detailed front and back views of this design. Notably, the dimensions of the design are carefully tailored, with a 150×75 mm^2, closely mirroring the size of a standard 6.6-inch smartphone.

Each of the six antennas, denoted as A1-A6 respectively, are sequentially positioned to optimize performance. To achieve minimal interference and crosstalk between ports, a sequential rotation technique is employed, ensuring that adjacent ports are precisely 90 degrees apart in polarization.

This configuration guarantees a (theoretical) zero crosstalk between the ports, enhancing the overall efficiency and reliability of the MIMO system.

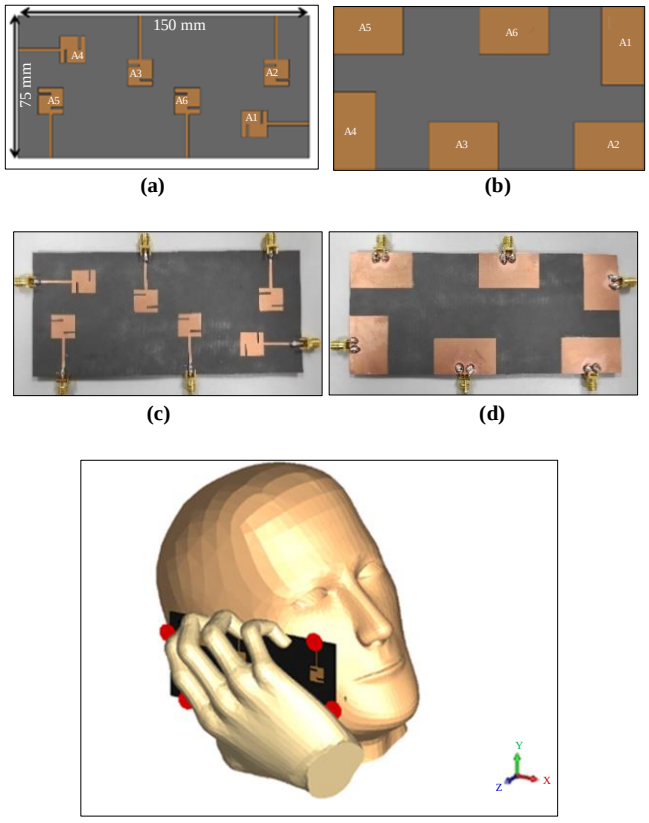

(a) (b)

(c) (d)

(e)

Fig. 3 MIMO design layouts (a) Front, (b) Back, (c) Front (fabricated), (d) Back (fabricated), and (e) SAR setup with hand-head phantom in CST

In addition to managing the polarization, measures are taken to prevent isolation issues between antenna pairs. Specifically, antennas A3 and A4, as well as A5 and A6, operate at the same polarization. To mitigate any potential isolation problems, we've maintained a 90 mm distance between these antenna pairs.

Figure 3(d) showcases the fabricated prototype, offering a representation of the design's front and back views. Finally, Figure 3(e) reveals the setup employed to calculate the SAR of the design, which is a crucial consideration in assessing smartphone performance. The SAR assessment ensures that the antenna design meets safety standards and does not expose users to excessive radiofrequency. The input power is considered as 10mW for this calculation. Next section (3) reveals the detailed results with an in-depth discussion of both SEA and 6×6 MIMO design.

3. Results and Discussion

The S_{11} responses for the three design stages (see Figure 2) are illustrated in Figure 4. In stage 1, no resonances (≤-10dB) are evident within the 1-12 GHz spectrum. Introducing the slots in stage 2 renders the response more frequency-selective; however, the objective of designing the antenna for the antenna centered around 3.5 GHz remains unmet. In the

concluding stage (3), the ground plane is truncated to form a PGP. The resulting S_{11} depicts a significant shift in response, showcasing a pronounced resonance at 3.4 GHz (-46dB). Furthermore, the -10dB BW stretches 2.9 - 4.3 GHz.

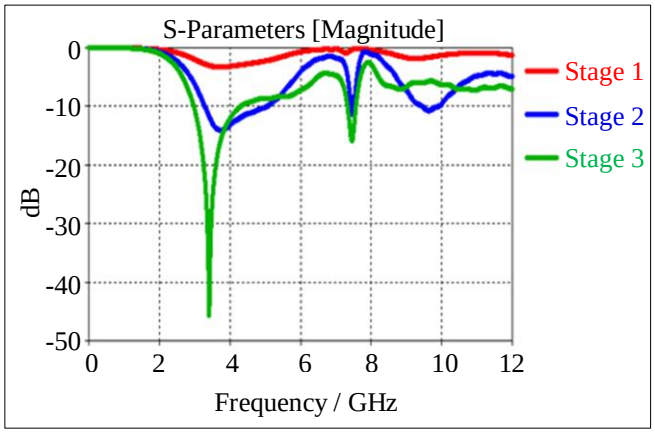

Fig. 4 S_{11} responses for different stages of design

Continuing with the SEA validation, Figure 5 presents the measured and simulated S_{11}, real & imaginary impedances, and the three- and two-dimensional (3-D & 2-D) radiation pattern responses. Figure 5(a) displays the S_{11} responses (both measured and simulated) across the 2 – 9 GHz spectrum of the proposed antenna. These measurements were performed using a Vector Network Analyzer (VNA), Agilent N5242A model. The results clearly demonstrate a notable concurrence between the measured and simulated S_{11} outcomes. Figure 5(b) showcases the same data but is restricted to the 2-5 GHz range for enhanced clarity. It is seen that the measured and the simulated S_{11} data are mainly in agreement. However, there are slight minor discrepancies that exist, potentially stemming from the fabrication process and SMA connector soldering.

For the measured S_{11}, the bandwidth commences at 3.1 GHz, marking a shift of approximately 200 MHz from the simulated data. A similar offset is discernible at the higher end of the spectrum, with the measured S_{11} crossing the -10 dB mark at 4.53 GHz, diverging from the simulated result. From Figure 5(c), it is seen that at 3.45GHz, the antenna has a zero imaginary impedance along with a 50 Ω real value (Zant = 50 + j0 Ω). This also indicates the low-loss nature of the design. Moreover, Figures 5(d), and 5(e) illustrates the radiation characteristic of the SEA. Figure 5(d) reveals the 3-D pattern response at 3.5GHz, and it is observed that radiation is mainly on the x-y plane, which proves the omni-direction pattern of the SEA. Again, Figure 5(e) shows the 2-D phi = 0 and phi = 90 patterns, which also supports the omnidirectional nature of the SEA design.

Moving on to the responses for the 6 × 6 MIMO design, Figure 6 reveals the measurement setup (Figures 6(a) & 6(b)) and the measured & simulated S-parameters (isolation) between the ports (Figures 6(c)-Figure 6(h)). To analyze the isolation and assess the performance of the proposed array it has great importance. To measure the 6-port device, three different measurements are taken to get all the desired isolation results. Each time, the other unmeasured MIMO ports are terminated with a 50 Ω termination load. In any MIMO design, the S-parameters between the ports are considered indicative of the isolation between them. For example, the S12/S21 response implies the isolation between port 1 and port 2, and so on.

Figure 6(c) comprises the simulation responses of S21, S31, S41, S51, and S61, whereby Figure 6(d) reveals the measured responses, indicating the isolation of port 1 from the other 5 ports. The measured and simulated responses show strong alignment, indicating good agreement between the two. Most of the responses are below the -27 dB level.

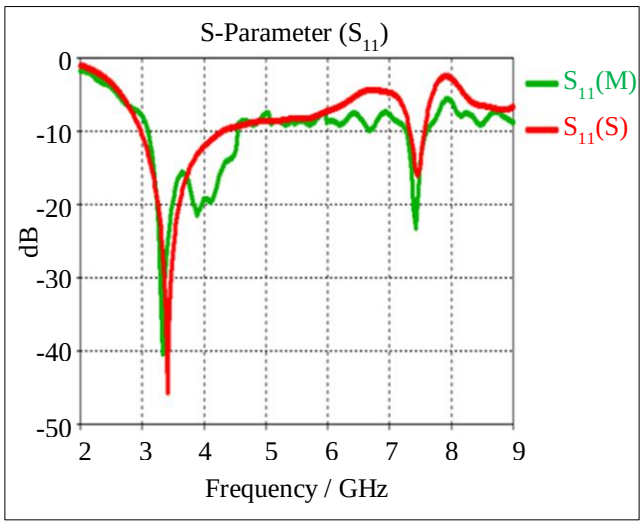

(a) S_{11} response of 2-9 GHz

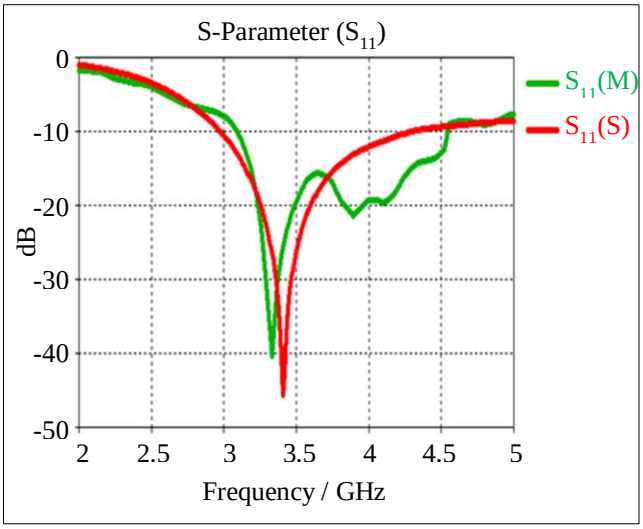

(b) S_{11} (2-5 GHz)

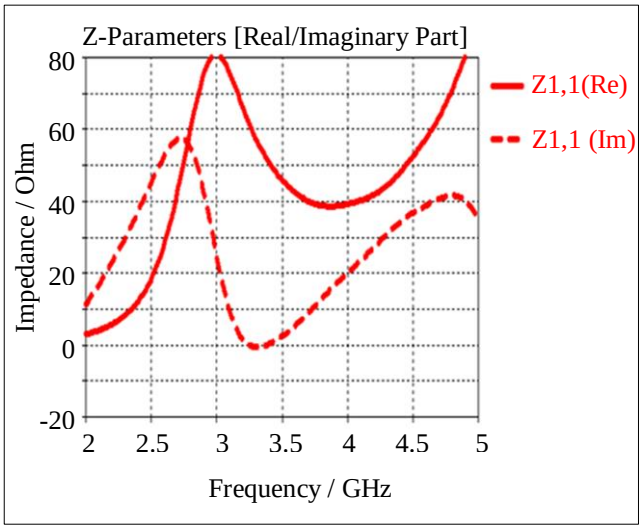

(c) Real and Imaginary Impedance

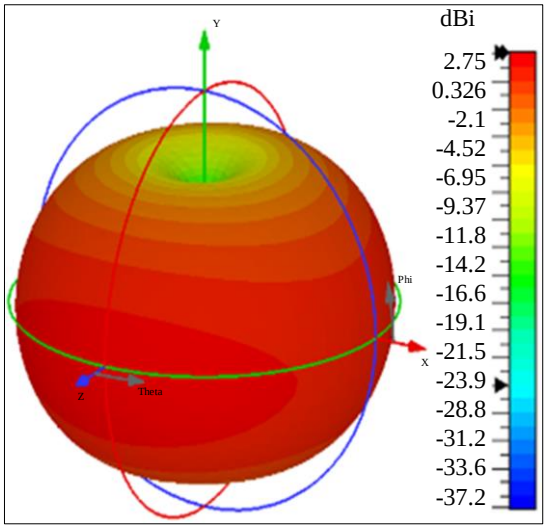

(d) 3-D radiation pattern

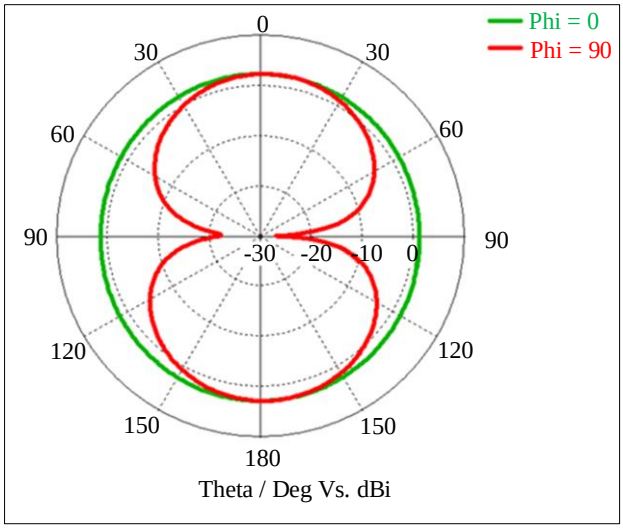

(e) 2-D radiation pattern (phi = 0 and 90)

Fig. 5 Impedance, S-parameter, VSWR, and radiation parameter of SEA design

(a) VNA measurement setup

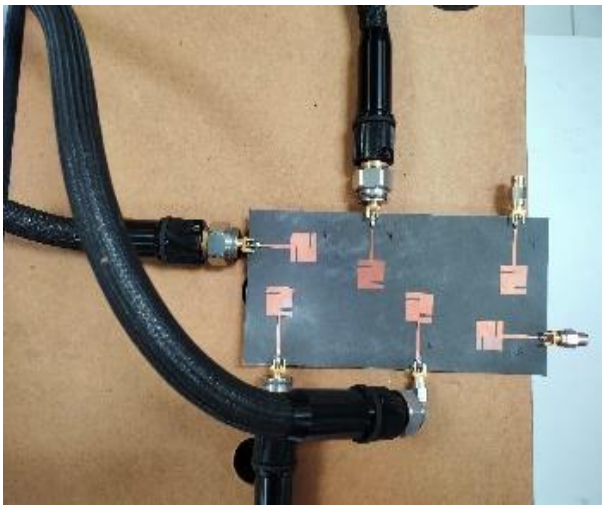

(b) Connection at ports

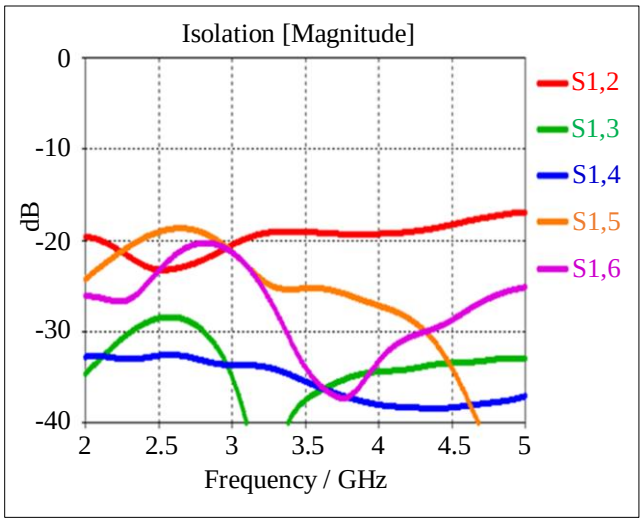

(c) Simulated

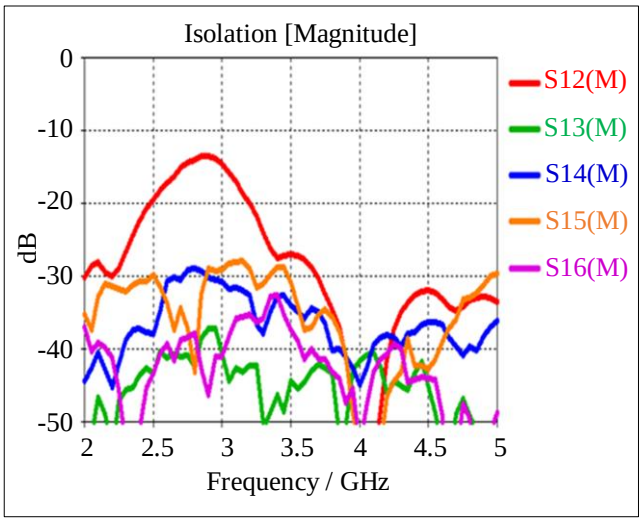

(d) Measured

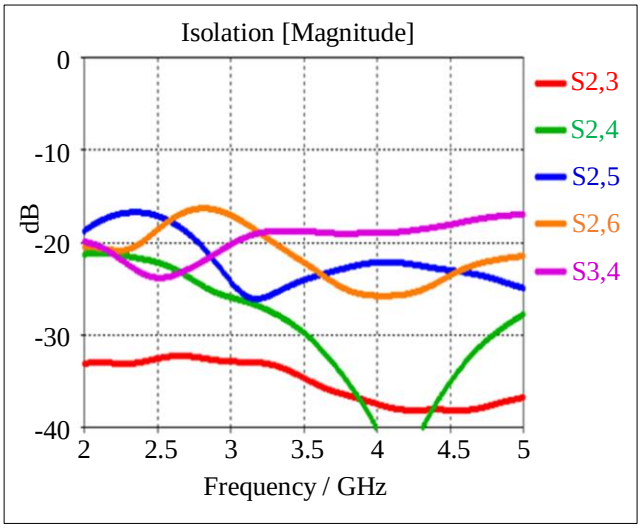

(e) Simulated

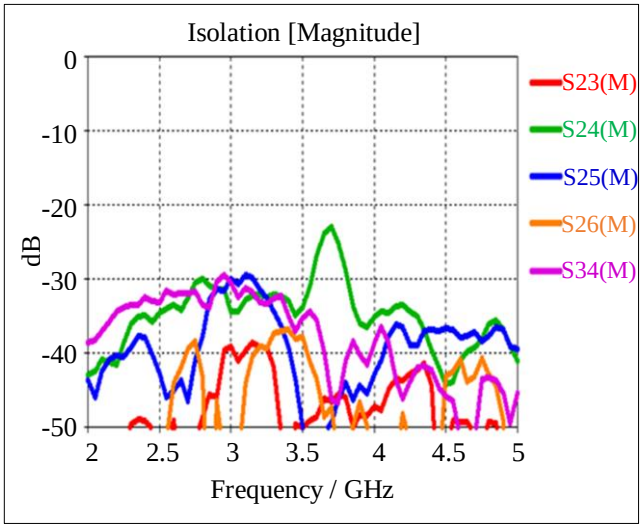

(f) Measured

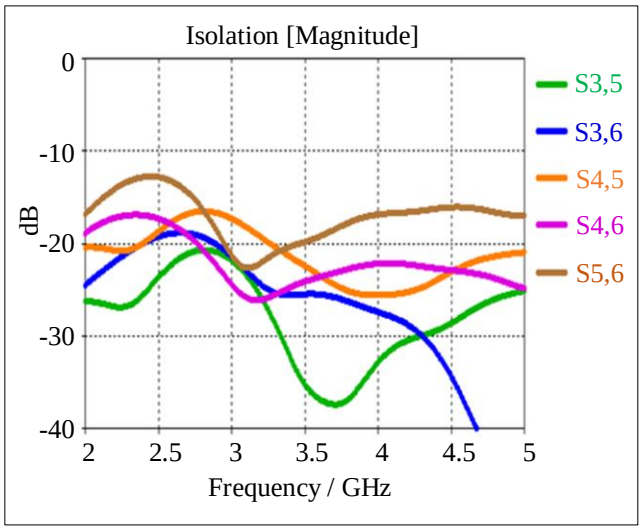

(g) Simulated

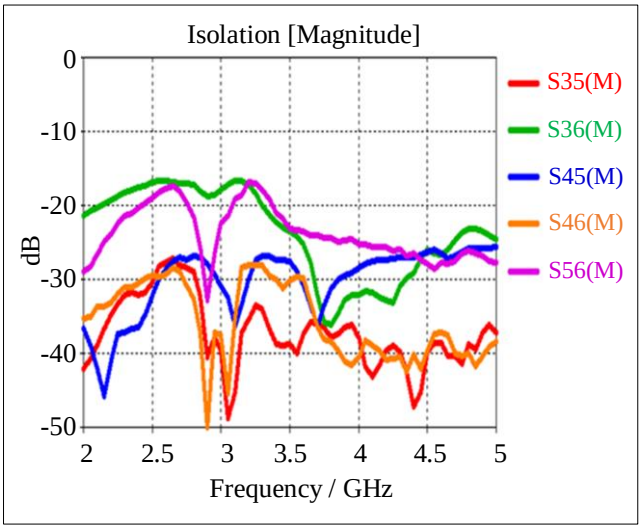

(h) Measured

Fig. 6 The isolation (S-parameters) between ports

However, we observe that for measured S_{21}, the value reaches as high as -17.3 dB, but it falls below -20 dB from 3.2 GHz until the end of the BW. Considering that the standard minimum isolation is ≤ -15 dB between any ports of the MIMO design [5], it can be concluded that the response still complies well with the standard. Furthermore, Figure 6(e), and 6(f) shows the isolations between port 2 with other ports. Also, it reveals the isolation of port 3 with port 4 (S_{34}). Notably, only S_{24} falls within the -20 dB to -30 dB range, while the rest exhibit isolation levels below -30 dB. This demonstrates the high quality of the design.

A similar scenario can be observed in Figure 6(g), and 6(h), which comprises the simulated and measured isolation responses respectively between port 4 & 5 (S_{45}), port 5 & 3 (S_{35}), port 6 & 3 (S_{36}), and port 6 & 5 (S_{56}), where most the isolation values between ports remain below -30 dB. However, only S_{56} and S_{36} go as high as -16.6 dB. In summary, it can be confidently stated that the isolation performance of this design is highly satisfactory. Two additional parameters, ECC and DG of the MIMO, are estimated by using CST MWS with the help of equations (3) and (4) (see Figure 7(a), and Figure 7(b)) [5].

$$ECC_{xy} = \frac{\left|S_{xx}^{*}S_{xy}+S_{yx}^{*}S_{yy}\right|^{2}}{\left(1-\left(|S_{xx}|^{2}+|S_{xy}|^{2}\right)\right)\left(1-\left(|S_{xx}|^{2}+|S_{yx}|^{2}\right)\right)} \quad (3)$$

$$DG_{xy} = 10\sqrt{1-\left|ECC_{xy}\right|^{2}} \quad (4)$$

Here, x = 1, and y = 2, 3, 4, 5, and 6. In theory, a lower ECC indicates better MIMO performance. From Figure 7(a), it is evident that the ECC value goes very low, around 0.0001, for most of the working BW of the design. At the beginning of the BW (3.1 GHz), the ECC is around 0.0025, and for the whole BW, the value never exceeds 0.004. In Figure 7(b), the DG consistently stays around 10 throughout the bandwidth, never dropping below 9.98.

In Figures 7(c), and 7(d), measurements that were conducted in an anechoic chamber are displayed. Figure 7(e) and 7(f) illustrate the simulated & the measured values for the TE and the RG, respectively. From Figure 7(e), it can be observed that the simulated TE peaks at 95%, while the measured value achieves a maximum of 80%, indicating a 15% difference between the two.

This variation could potentially arise from fabrication or soldering discrepancies. Similarly, the peak RG is registered at 5.53 dBi (simulated) at 4.5 GHz and 5.44 dBi (measured) at 3.3 GHz. This difference could be attributed to the previously mentioned factors. Nonetheless, the values for both these parameters follow a consistent trend. Figure 8 comprises the radiation pattern responses of the proposed MIMO antenna. Figure 8(a), and 8(b) comprise the combined results of 3-D and 2-D antenna radiation patterns, respectively, calculated by the postprocessing section in CST-MWS. Similarly, Figure 8(c), and Figure 8(d) reveals the 3-D radiation patterns of the port 1 and 2, respectively. Here, only port 1 and port 2 have been chosen for measurement, as the other ports resemble them.

It is evident that at port 1, the 3-D pattern radiates mostly on the x-y plane, with some lower radiation strength points. To confirm the radiation characteristics, a 2-D analysis has been done. Figure 8(e) reveals the 2-D radiation patterns (for Phi = 00 and Phi = 900) for port 1. It is evident that, for both planes, the antenna radiates well and follows the 3-D pattern with less radiation at 0 and 180 degrees of the antenna plane. Similarly, we observe port 2's 2-D radiation patterns in Figure 8(f).

It is clear from the 3-D pattern that port 2 radiates the most on the y-z plane, with two low radiating points at 0 and 180 degrees of the antenna plane. The phi = 00 and phi = 900 2-D radiation plots also confirm the same situation. Investigating the measured radiation patterns for each port shows the antenna radiates effectively in a 360-degree pattern, giving the all-directional propagation essential for robust mobile communication.

Next, the same antenna was exported and fitted inside a hand-head phantom model using CST MWS to analyze human interaction and the effect on the radiation pattern, as well as to estimate the SAR leaked to the human body. Figures 9 and 10 reveal the responses of the radiation pattern and the SAR values, respectively, at each port for this scenario. The estimation is done at 3.5 GHz.

Figures 9(a) to 9(f) represent the 3-D radiation pattern responses for port 1 – port 6, respectively. It is observed that ports 1, 3, and 6 radiate the beam in front of the hand-head phantom, while ports 1, 4, and 5 radiate at the backside of the phantom.

For each radiation pattern, it is clearly visible that the radiation is outwards from the hand-head, indicating low radiation power towards the body and less loss during communication between the mobile device and the nearest cell tower. Overall, it is also clear that the MIMO can communicate in all directions of the radiation.

Lastly, Figures 10(a) to 10(f) represents the SAR responses for ports 1 – port 6, respectively, at 3.5GHz. The lowest SAR value is 0.094 W/Kg (port 2), and it goes as high as 0.41 W/Kg at port 3. For ports 1, 4, 5, and 6, the SAR is 0.13, 0.29, 0.11, and 0.20 W/Kg, respectively. The standard for maximum SAR is 1.6 W/Kg and 2.0 W/Kg for 1g and 10g mass, respectively [4]. Based on this, it is evident that the SAR is very well within the accepted standard and safe for use in smartphone communication for 5G.

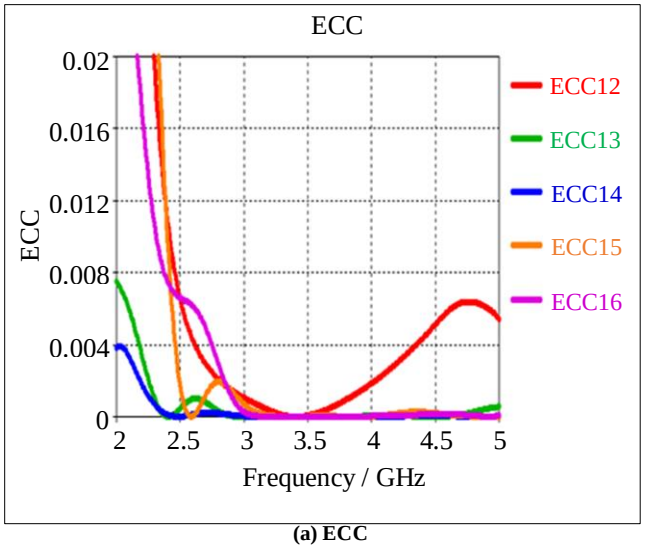

(a) ECC

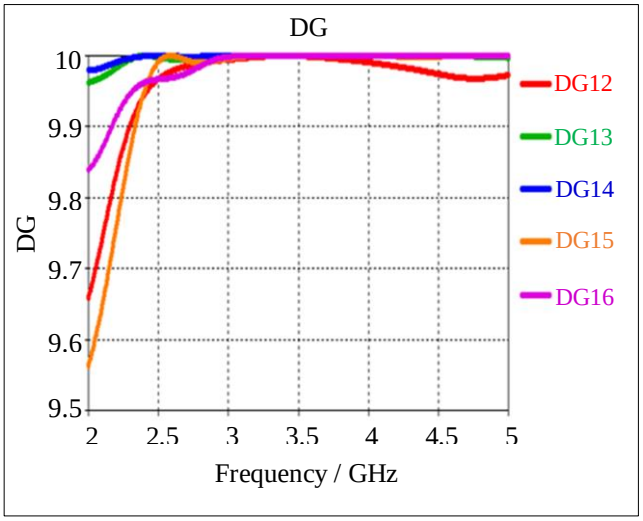

(b) DG

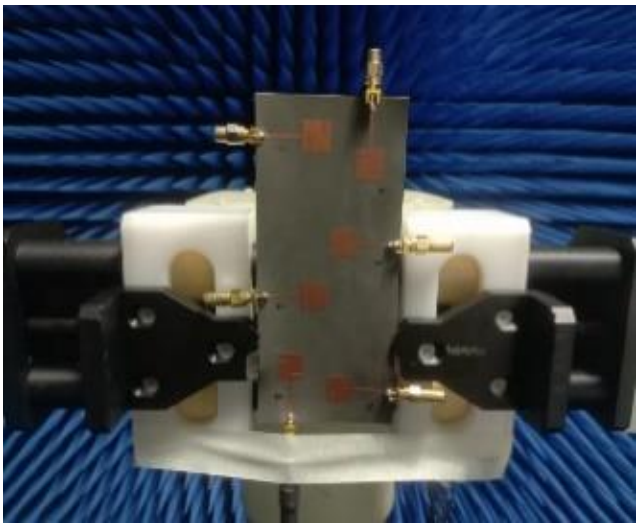

(c) Anechoic chamber setup

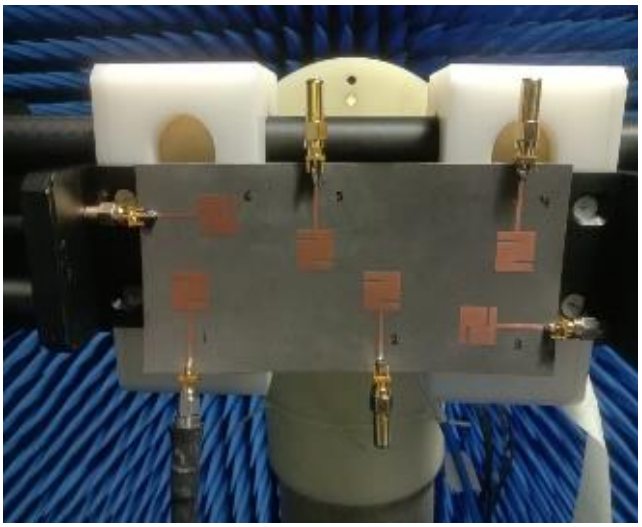

(d) Antenna connection

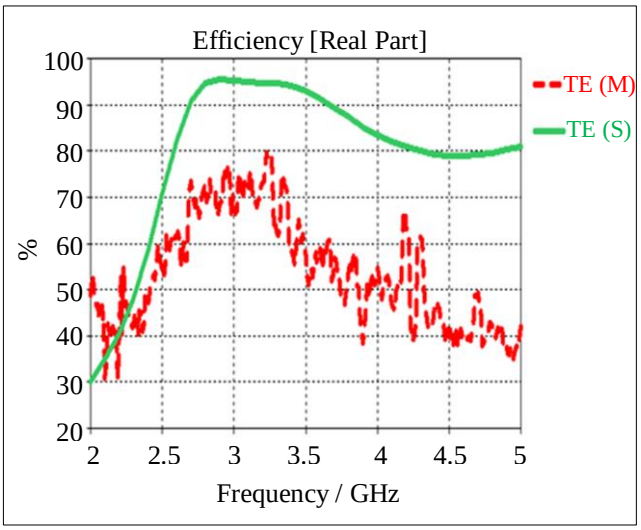

(e) TE

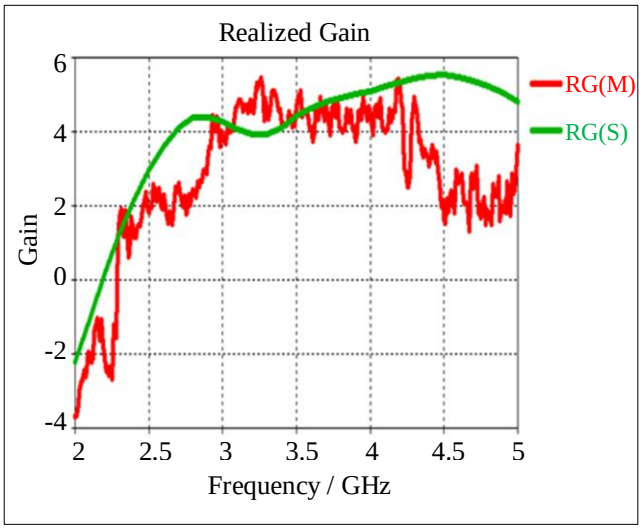

(f) RG

Fig. 7 The ECC, DG, TE, and RG of the proposed design

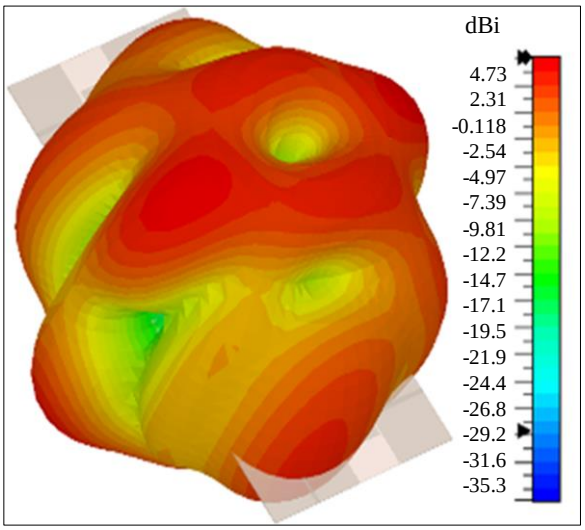

(a) 3-D (combined)

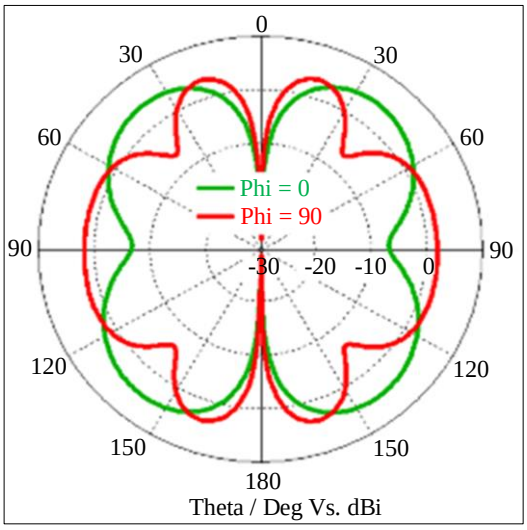

(b) 2-D (combined)

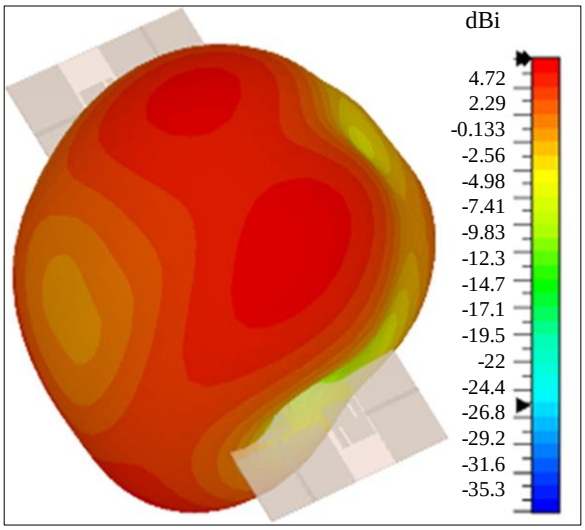

(c) 3-D (Port 1)

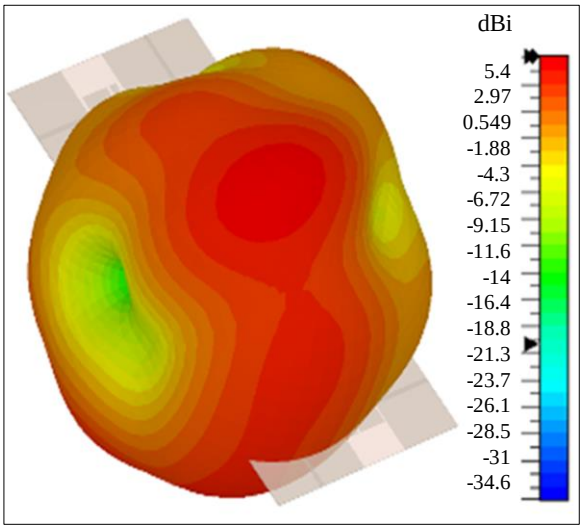

(d) 3-D (Port 2)

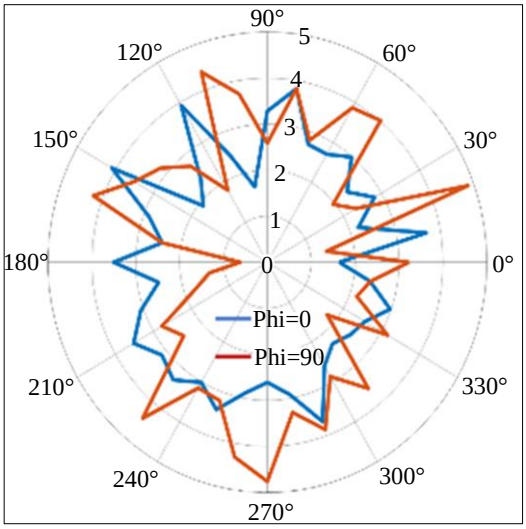

(e) 2-D (Port 1)

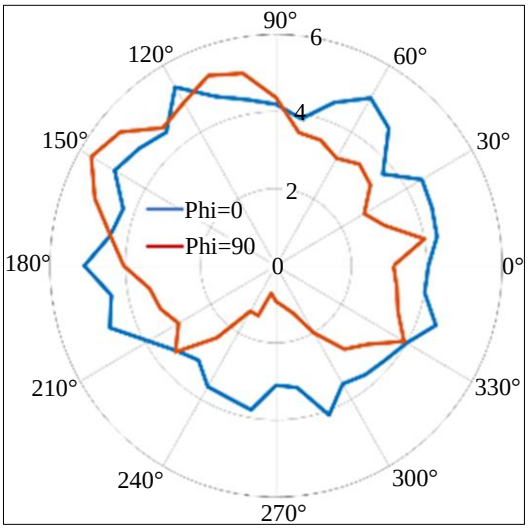

(f) 2-D (Port 2)

Fig. 8 The port 1 and port 2, 3-D and 2-D radiation pattern

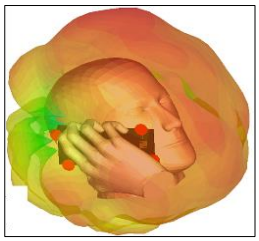

(a) port 1

(b) port 2

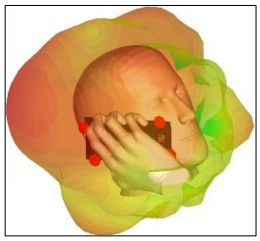

(c) port 3

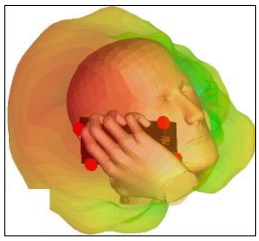

(d) port 4

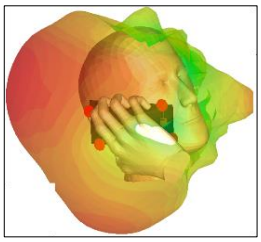

(e) port 5

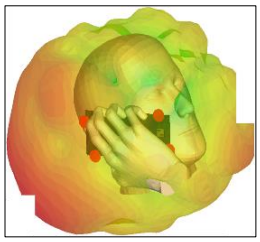

(f) port 6

Fig. 9 The effect of the hand-head phantom on radiation pattern

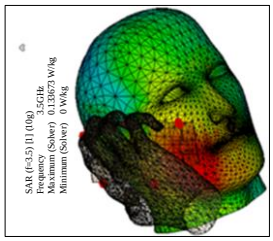

(a) port 1

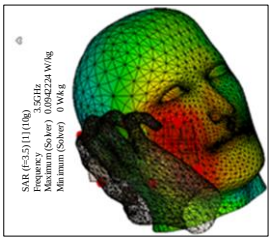

(b) port 2

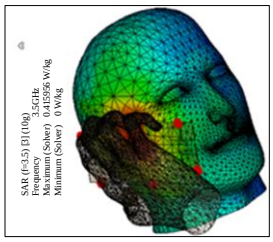

(c) port 3

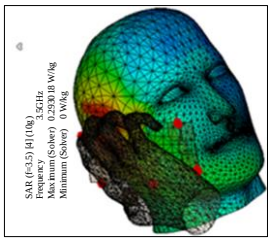

(d) port 4

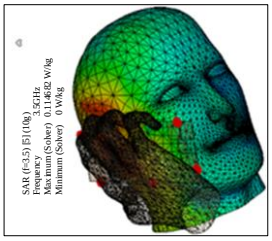

(e) port 5

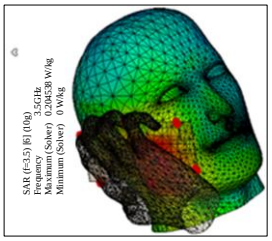

(f) port 6

Fig. 10 SAR calculation using hand-head phantom using CST MWS

4. Conclusion

In conclusion, it can be stated that a 6×6 MIMO array meticulously designed for 5G (sub-6 GHz) smartphone and wireless applications is introduced in this work. The utilization of the PGP configuration, along with the integration of a single-element dual rectangular slotted monopole antenna, has yielded an ultra-wideband response.

This design is tailored to integrate with modern 6.6-inch display smartphones. This proposed design operates within the frequency range of 3.1 - 4.53 GHz and exhibits a -10 dB BW of 1.43 GHz, which covers the mid 5G band (3.5GHz). With port-to-port isolation exceeding -16.6 dB, a maximum RG of 5.44 dBi, and the highest TE of 80%, it demonstrates its prowess in wireless communication. Comprehensive far-field radiation patterns across all six ports attest to its robustness. Furthermore, the proposed design maintains an ECC consistently below 0.004, and the DG is always above the value of 9.98, affirming its reliability across diverse operational scenarios as a MIMO array. The SAR testing validates compliance with MIMO standards, with values as low as 0.094 W/kg (10g mass), underscoring its commitment to safety and regulatory requirements.

Acknowledgments

This research is fully funded by the Fundamental Research Grant Scheme (FRGS) from the Ministry of Higher Education (MOHE) Malaysia with grant No. FRGS/1/2021/TK0/UTEM/02/34 in Technical University of Malaysia Malacca (UTeM).

References

[1] Arun Pant, Manish Singh, and Manoj Singh Parihar, "A Frequency Reconfigurable/Switchable MIMO Antenna for LTE and Early 5G Applications," *AEU - International Journal of Electronics and Communications*, vol. 131, 2021. [CrossRef] [Google Scholar] [Publisher Link]

[2] Jingli Guo et al., "Side-Edge Frame Printed Eight-Port Dual-Band Antenna Array for 5G Smartphone Applications," *IEEE Transactions on Antennas and Propagation*, vol. 66, no. 12, pp. 7412-7417, 2018. [CrossRef] [Google Scholar] [Publisher Link]

[3] Naveen Kumar, and Rajesh Khanna, "A Two Element MIMO Antenna for Sub-6 GHz and mmWave 5G Systems Using Characteristics Mode Analysis," *Microwave and Optical Technology Letters*, vol. 63, no. 2, pp. 587-595, 2021. [CrossRef] [Google Scholar] [Publisher Link]

[4] Amany A. Megahed et al., "5G Millimeter Wave Wideband MIMO Antenna Arrays with High Isolation," *EURASIP Journal on Wireless Communications and Networking*, vol. 2023, pp. 1-16, 2023. [CrossRef] [Google Scholar] [Publisher Link]

[5] A.K.M. Zakir Hossain et al., "A Planar 2×2 MIMO Antenna Array for 5G Smartphones," *International Journal of Advanced Computer Science and Applications*, vol. 12, no. 7, pp. 710-717, 2021. [CrossRef] [Google Scholar] [Publisher Link]

[6] Zhouyou Ren, and Anping Zhao, "Dual-Band MIMO Antenna with Compact Self-Decoupled Antenna Pairs for 5G Mobile Applications," *IEEE Access*, vol. 7, pp. 82288-82296, 2019. [CrossRef] [Google Scholar] [Publisher Link]

[7] Jianlin Huang et al., "A Quad-Port Dual-Band MIMO Antenna Array for 5G Smartphone Applications," *Electronics*, vol. 10, no.5, pp. 1-9, 2021. [CrossRef] [Google Scholar] [Publisher Link]

[8] Muhammad Ali Jamshed et al., "Dual Band and Dual Diversity Four-Element MIMO Dipole for 5G Handsets," *Sensors*, vol. 21, no. 3, pp. 1-13, 2021. [CrossRef] [Google Scholar] [Publisher Link]

[9] Vandana Yadav et al., "Dual and Wideband 6-Port MIMO Antenna for WiFi, LTE and Carrier Aggregation Systems Applications," *AEU - International Journal of Electronics and Communications*, vol. 162, 2023. [CrossRef] [Google Scholar] [Publisher Link]

[10] Mohamed M. Morsy, "Compact Eight-Element MIMO Antenna Array for Sub 6 GHz Mobile Applications," *SN Applied Sciences*, vol. 5, pp. 1-7, 2023. [CrossRef] [Google Scholar] [Publisher Link]

[11] Naser Ojaroudi Parchin et al., "An Efficient Antenna System with Improved Radiation for Multi-Standard/Multi-Mode 5G Cellular Communications," *Scientific Reports*, vol. 13, pp. 1-7, 2023. [CrossRef] [Google Scholar] [Publisher Link]

[12] Haroon Ahmed et al., "Sub-6 GHz MIMO Antenna Design for 5G Smartphones: A Deep Learning Approach," *AEU - International Journal of Electronics and Communications*, vol. 168, 2023. [CrossRef] [Google Scholar] [Publisher Link]

[13] Zhonggen Wang et al., "Design of MIMO Antenna with Double L-Shaped Structure for 5G NR," *Symmetry*, vol. 15, pp. 1-13, 2023. [CrossRef] [Google Scholar] [Publisher Link]

[14] Muhammad Zahid et al., "Ten-Port MIMO Inverted-F Antenna for LTE Bands 43/48/49 Bands Smartphone Applications," *Electronics*, vol. 12, no. 19, pp. 1-14, 2023. [CrossRef] [Google Scholar] [Publisher Link]

[15] Ji-Peng Jhuang, and Hsin-Lung Su, "A Compact 12 × 12 MIMO Loop Antenna for 5G Mobile Phone Applications," *International Journal of Microwave and Wireless Technologies*, pp. 1-11, 2023. [CrossRef] [Google Scholar] [Publisher Link]

[16] Chih Chung Lin et al., "Compact Sub 6 GHz Dual Band Twelve-Element MIMO Antenna for 5G Metal-Rimmed Smartphone Applications," *Micromachines*, vol. 14, pp. 1-17, 2023. [CrossRef] [Google Scholar] [Publisher Link]